




Original Paper

Can One-Run-Fixed-Arrhenius Kerogen Analysis Provide Comparable Organofacies Results to Detailed Palynological Analysis? A Case Study from a Prospective Mississippian Source Rock Reservoir (Bowland Shale, UK)

Sarah M. Newport ^{1,5}, Jan A. I. Hennissen,² James P. Armstrong,³ Kevin G. Taylor,¹ Leo P. Newport,⁴ and Edward Hough²

Received 15 May 2019; accepted 13 August 2019
Published online: 26 August 2019

Organofacies analysis, a fundamental component within source rock appraisal based on the study of kerogen within a source rock, is typically produced from microscopy (palynological) and geochemical (kerogen kinetic) data, both of which are costly to acquire. One-Run-Fixed-Arrhenius (ORFA) kerogen kinetic analysis based on Rock-Eval pyrolysis offers a substantially cheaper kinetic dataset. Here, ORFA and palynological analyses are compared in organofacies characterization of a prospective Mississippian source rock reservoir (Bowland Shale, UK). Two-end-member organofacies were determined based on the abundance of the 56 kcal/mol activation energy peak derived from ORFA data: absence (< 5%) indicating ‘organofacies A’ containing the highest proportion of algal material (Type I kerogen); and presence (> 15%) indicating ‘organofacies B’ containing the highest proportion of sporomorphs (Type II kerogen). A mud-dominated slope setting for the rock reservoir was also used to test the accuracy of organofacies analysis in determining depositional environment. Organofacies A found within lithofacies deposited from dilute waning density flows and hemipelagic suspension settling occurred between shelf edge, slope and basin. Organofacies B found within lithofacies deposited from dilute waning density flows, and low-strength cohesive debrites occurred only within the lower slope. This study demonstrates that ORFA kerogen kinetic analysis provides comparable net results to palynological analysis, enabling cheaper and faster organic characterization during initial source rock appraisal. However, caution must be exercised in drawing interpretations as to biological source(s), organic matter mixing and preservation state(s) without additional investigation using data from detailed palynological analysis.

KEY WORDS: Source rock, Organofacies, Kerogen kinetics, One-Run-Fixed-Arrhenius, Palynology, Bowland Shale.

¹School of Earth and Environmental Sciences, University of Manchester, Manchester M13 9PL, UK.

²British Geological Survey, Environmental Science Centre, Nicker Hill, Keyworth, Nottingham NG12 5GG, UK.

³Petroleum Systems Limited, 30 Linden Walk, Prestatyn, Denbighshire LL19 9EB, UK.

⁴Worcester Sixth Form College, Spetchley Road, Worcester WR5 2LU, UK.

⁵To whom correspondence should be addressed; e-mail: sarah.m.newport@manchester.ac.uk

INTRODUCTION

Within unconventional or conventional hydrocarbon exploration and appraisal, it is critical to characterize the source rocks within the petroleum system. Source rock appraisal includes determining the distribution of rock properties based on both depositional and post-depositional processes (e.g.,

Ross and Bustin 2009; Aplin and Macquaker 2011; Fishman et al. 2012; Macquaker et al. 2014), to the organic matter content (e.g., Passey et al. 1990; Creaney and Passey 1993; Tyson 2004), type (e.g., Tissot et al. 1974; Tissot and Welte 1984; Katz 1995; Hackley and Cardott 2016), maturity (e.g., Raiswell and Berner 1987; Bernard et al. 2012) and ultimate generation potential (e.g., Pepper and Corvi 1995; Behar et al. 1997; Waples 2000; Ross and Bustin 2008). The integrated study of the kerogen [the fraction of sedimentary organic matter that is non-extractable in organic solvents (Durand 1980)] contained within a source rock using both microscopy and geochemical techniques, as defined in the concept of ‘organofacies,’ is an essential tool for hydrocarbon source rock appraisal (e.g., Roger 1979; Cornford et al. 1980; Jones 1987; Peters and Cassa 1994; Tuweni and Tyson 1994; Pepper and Corvi 1995; Evenick and McCain 2013). Organofacies analysis enables a geoscientist to make accurate predictions of the likely occurrence and lateral variability of hydrocarbon source potential as a function of depositional environment (Jones and Demaison 1982; Tyson 1987, 1995).

Two techniques are commonly used to produce an organofacies analysis: kerogen kinetic data and palynological (palynofacies) analysis. Palynofacies analysis involves the integrated study of all aspects of the kerogen assemblage based on transmitted light petrographic analysis: identification of the individual particulate components, assessment of their absolute or relative proportions and preservation states (Tyson 1995).

Kerogen kinetic analysis involves the laboratory maturation of organic matter in source rock samples in order to determine the kinetic controls (i.e., the Arrhenius equation (Eq. 1) gives the dependence of the rate constant of a chemical reaction (k) on the absolute temperature (T , Kelvin), a pre-exponential factor (A) and other constants of the reaction: the activation energy (E_a) and the universal gas constant (R)) on the first-order reactions which occur (Tissot and Espitalie 1975; Wood 2019).

$$k = Ae^{-E_a/RT} \quad (1)$$

Various laboratory methods have been proposed to predict the thermal behavior of organic matter during burial maturation, open-system pyrolysis (such as Rock-Eval™, e.g., Waples 2000), closed-system isothermal pyrolysis (such as hydrous pyrolysis, e.g., Lewan et al. 1979; Lewan and Ruble

2002), microscale sealed vessel (MSSV) pyrolysis (e.g., Horsfield et al. 1989) or gold tube reactor pyrolysis (e.g., Behar et al. 1992). Significant debate occurs within the scientific community surrounding the reliability of kinetics determined using open- vs. closed-system pyrolysis (e.g., Burnham et al. 1988; Schenk and Horsfield 1993; Ritter et al. 1995; Lewan and Ruble 2002; Peters et al. 2015; Waples 2016). The method of inverting kerogen kinetics from pyrolysis data using a distribution of activation energies focused on a fixed pre-exponential factor has also recently been questioned (Wood 2019), suggesting that a distribution of Arrhenius reactions with variable E_a and A values provides a more realistic representation of kerogen reaction kinetics.

This paper aims to establish whether organofacies interpretations based on kerogen kinetics derived from the One-Run-Fixed-Arrhenius (ORFA) technique proposed by Waples et al. (2002), Waples and Nowaczewski (2013) and Waples (2016) are directly comparable to organofacies interpretations based on palynofacies analysis (Tyson 1995). The study material is a continuous core (Marl Hill: MHD 11; British Geological Survey reference number SD64NE/20) from an active exploration play, the Bowland Shale Formation (Andrews 2013; Clarke et al. 2018), which has previously undergone detailed sedimentological analysis (Newport et al. 2017). Organofacies interpretations based on both ORFA and palynological analysis were used to (i) describe the dominant organofacies in the Bowland Shale and (ii) identify whether there is a discernible relationship between organofacies and depositional setting (previously described lithofacies and facies associations).

Geological Setting of the Bowland Shale Formation

During the Carboniferous (347–318 Ma; Fig. 1) a shallow epicontinental seaway extended across the Laurussian continent. The equatorial Pennine Province (northern England, UK) formed a series of interconnected basins between emergent land (to the north the Southern Uplands High; to the south the Wales–London–Brabant High) as a result of back-arc rift extension related to the Variscan Orogeny (410–280 Ma; Fraser and Gawthorpe 1990; Davies 2008; Waters et al. 2011). The Bowland Basin (the focus of this study), a complex NE–SW-trending fault-controlled half-graben within the larger

Craven Basin, had three main phases of rifting (initiation in the late Devonian–Tournaisian; Chadian–Arundian; Asbian–Brigantian; Figure 1; Gawthorpe 1987; Arthurton et al. 1988; Riley 1990; Fraser and Gawthorpe 2003). Deposition within the basin evolved from carbonate-dominated during the Viséan (carbonate ramp which evolved to a carbonate-rimmed shelf; Gawthorpe 1986) to clastic-dominated by the Serpukhovian (progradation of the Millstone Grit deltas from the north; Aitkenhead et al. 1992; Brandon et al. 1998; Kirby et al. 2000; Kane et al. 2010). The Bowland Shale is similar to the Barnett Shale play of the Fort Worth Basin (USA) with both being mid-Carboniferous calcareous organic-rich shales (Andrews 2013; Hough et al. 2014), although critically it differs with respect to its thickness (over 500 m or 1600 ft in some localities), its paleogeography (accumulation in a series of smaller basins) and its geological history (complex including phases of basin inversion). In addition, the hydrocarbon potential of the Bow-

land Shale differs from the Barnett Shale of the Fort Worth Basin as significant areas within the Pennine Province do not have sufficient thermal maturity for the organic matter of the Bowland Shale (and its lateral equivalents) to generate gas (Jarvie et al. 2007; Metcalfe and Riley 2010).

The Marl Hill 11 Borehole

The Marl Hill 11 borehole [SD 6833 4683], currently stored by the British Geological Survey at Keyworth (UK), was collected in 1981 as part of the Marl Hill drilling program conducted by BP Mineral International Ltd. The core consists of a 300.58 m succession containing the following stratigraphic intervals: Worston Shale Group (comprising of the Hodder Mudstone Formation, Limekiln Wood Limestone Formation and Hodderense Limestone Formation) and Bowland Shale Group (comprising of the Pendleside Limestone Formation, Lower

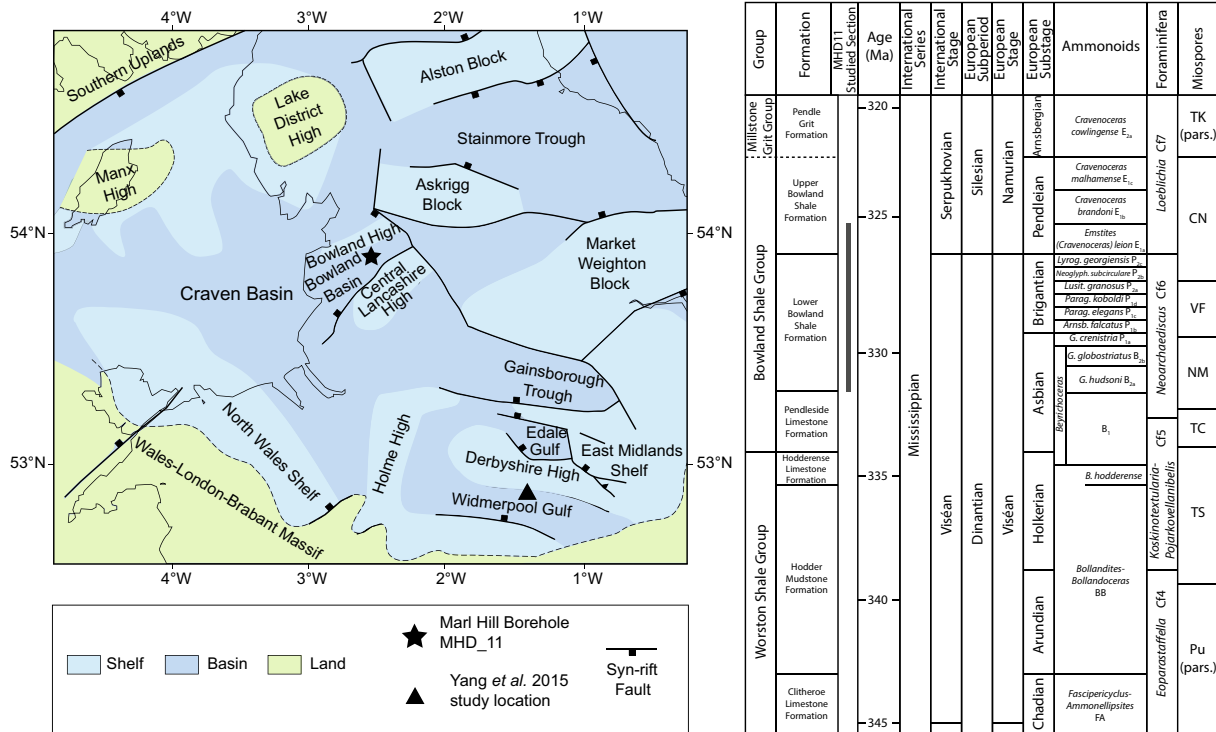


Figure 1. Mississippian paleogeography of northern England (UK) with modern geographical outline of the UK shown and stratigraphic column for the Bowland Basin (modified after Waters et al. 2009); ammonoid and foraminifera zones (after Riley 1993; Somerville 2008; Waters and Condon 2012); palynozonation (after Owens 2004). TK = *Mooreisporites trigallerus*—*Rotaspora knoxi* zone; CN = *Reticulatisporites carnosus*—*Bellisporites nitidus* zone; VF = *Tripartites vetustus*—*Rotaspora fracta* zone; NM = *Raistrickia nigra*—*Triquitrites marginatus*; TC = *Perotrilites tessellatus*—*Schulzospira campyloptera*; TS = *Knoxisporites triradiatus*—*Knoxisporites stephanephorus*; Pu = *Lycospora pusilla*. The black star denotes the location of the Marl Hill 11 (MHD 11) borehole used within this study.

Bowland Shale Formation and Upper Bowland Shale Formation; Fig. 1; Aitkenhead et al. 1992). This interval equates to the Craven Group, consisting of the Hodder Mudstone Formation, Hodderense Limestone Formation, Pendleside Limestone Formation and Bowland Shale Formation of Waters et al. (2011). Within this study, the former stratigraphic nomenclature is used to allow correlation with older, established stratigraphies (i.e., the seismic stratigraphy of Fraser and Gawthorpe 2003). Within the cored Bowland Shale interval, three marine bands are present: B_{2b}, *Goniatites globostriatus* (*Beyrichoceras* biozone, Upper Asbian), P₂, *Sudeticerus* (Upper Brigantian) and E_{1a}, *Emstites (Cravenoceras) leion* (Lower Pendleian) (Figs. 1 and 2; Riley 1988; Aitkenhead et al. 1992). The focus of this study is the succession from 5 to 68 m consisting solely of the Bowland Shale For-

mation. The core is slabbed, and recovery of the core in the interval from 5 to 68 m is c. 92%.

Previous studies of the MHD 11 core have established six lithofacies, comprising calcareous claystone, calcareous mudstone, argillaceous mudstone, calcareous siltstone, calcareous sandy mudstone and matrix-supported carbonate conglomerate, present in core MHD 11 (Newport et al. 2017). Three facies associations were identified: a sediment-starved slope, a slope dominated by turbidites and a slope dominated by debrites. Conditions of sediment starvation on the slope occurred during flooding of the contemporaneous shelf, when shorelines and loci of active clastic and carbonate sedimentation were furthest away from the slope, while the transition toward a slope dominated by turbidites and then debrites occurred during normal or forced shoreline progradation toward the shelf margin (Newport et al. 2017).

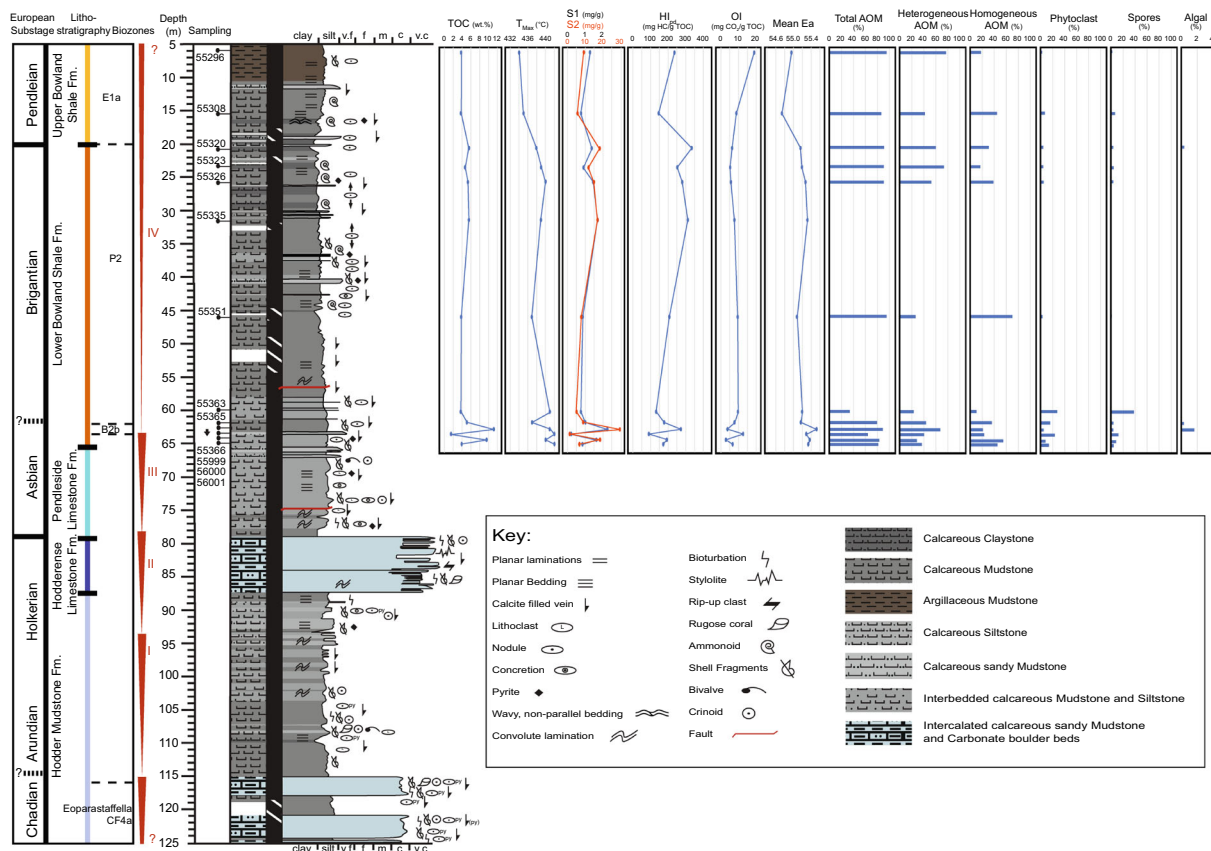


Figure 2. Lithostratigraphical, geochemical and palynological results of the Marl Hill (MHD 11) core material, including lithofacies features, sample locations, interpreted sequence stratigraphy (after Newport et al. 2017) and biozones (after Riley 1988).

METHODOLOGY

Sedimentological Analysis

The core was logged for visible textural (grain size) and compositional changes, sedimentary features and fossil content at a 10 cm resolution. Based on macroscopic observation, the core was subdivided into lithofacies using the classification proposed by Lazar et al. (2015) and previously described for a larger dataset by Newport et al. (2017). Distinction was primarily based on grain size with sediments containing > 66% grains smaller than 8 μm defined as claystones; > 66% grains 8 to 32 μm defined as mudstones; and > 66% grains 32 to 62.5 μm defined as siltstones. In addition, compositional modifiers 'siliceous,' 'calcareous' and 'argillaceous' were used when visual estimates determined > 50% of the sediment contained quartz, carbonate or clay.

Thin section analysis was conducted on all 13 samples taken from the Bowland Shale Formation, chosen to represent the different facies observed within the Newport et al. (2017) study, while total organic carbon (TOC) analysis ensured samples chosen were organically rich. All samples were prepared for polished (uncovered) thin sections normal to principal bedding orientation. Optical microscopy was undertaken using a Nikon Eclipse LV100NPOL microscope fitted with a Nikon DS-Fi2 camera; routine study was conducted using 50 \times , 100 \times and 200 \times magnification.

Total Organic Carbon (TOC) Analysis

Total organic carbon (TOC) was measured using a Leco CS230 carbon analyzer, calibrated using Leco supplied certified carbon standards appropriate to the carbon content of the samples. Prior to analysis, a portion of each sample was decalcified using 5 M hydrochloric acid and rinsed five times with distilled water. Accelerators (Iron chip, 0.7 g and Tungsten, \sim 1.5 g) were used. Samples were then heated to c. 1500 $^{\circ}\text{C}$ in an oxygen atmosphere within an induction furnace, and the resulting CO_2 was then quantified using an infrared detector.

Rock-Eval Analysis

A Wildcat HAWK pyrolyzer configured in standard mode was used to conduct the analysis of

samples. For each sample, between 50 and 100 mg of powdered whole rock was pyrolyzed in an inert helium atmosphere from 180 to 600 $^{\circ}\text{C}$, using a ramp rate of 25 $^{\circ}\text{C}$ per min. A flame ionizing detector (FID) was used to measure the mass of hydrocarbon vapors produced at 300 $^{\circ}\text{C}$ (thermally vaporized free hydrocarbons (HC); expressed as mg HC/g rock; S_1 peak of the pyrogram). The temperature was then increased from 300 to 550 $^{\circ}\text{C}$ to crack non-volatile organic matter (i.e., kerogen; expressed as mg HC/g rock; producing the S_2 peak of the pyrogram, CO_2 and water). The T_{max} , a proxy for thermal maturity, was determined from the temperature at which the S_2 peak reaches maximum generation. Thermal maturity values determined from T_{max} values within the dataset are consistent with reported conodont color alteration indices (CAI) of 2 to 2.5 for the region of the Marl Hill borehole (Metcalf and Riley 2010). The CO_2 generated during the thermal breakdown of kerogen was recorded as the S_3 peak of the pyrogram. Additional Rock-Eval parameters were calculated following Tissot and Welte (1984): (1) hydrogen index, $\text{HI} = (S_2/\text{TOC}) \times 100$; (2) oxygen index, $\text{OI} = (S_3/\text{TOC}) \times 100$; (3) production index, $\text{PI} = S_1/(S_1 + S_2)$; (4) pyrolysate yield, $\text{PY} = S_1 + S_2$. TOC values were derived solely from the Leco carbon analyzer. All experimental procedures for Rock-Eval analysis follow the Norwegian Industry Guide to Organic Geochemical Analyses (NIGOGA), 4th Edition. A standard (Jet-Rock 1) was run as every tenth sample and checked against the acceptable range given in NIGOGA (Weiss et al. 2000).

One-Run-Fixed-Arrhenius (ORFA) Kerogen Kinetic Analysis

The petroleum generation kinetics of all 13 samples was determined using one-run, open-system pyrolysis experiments with a single heating rate (of 25 $^{\circ}\text{C}$ per min) and fixed (pre-exponential) frequency factor (A of $2 \times 10^{14} \text{ s}^{-1}$; Eq. 1; Waples and Nowaczewski 2013; Waples 2016). The fixed single value of A used within this study follows the method of Waples and Nowaczewski (2013) where the fixed A value was determined from the distribution of A factors by allowing A and E_a to vary freely; the median and mean values for $\log A$ both yield a value for A near $1.6 \times 10^{14} \text{ s}^{-1}$ which was then rounded up to the value of $2 \times 10^{14} \text{ s}^{-1}$. The influences of A and E_a cannot be separated when using only a single

pyrolysis run, requiring the use of a fixed value for A to be used. However, once A is specified a full activation energy (E_a) distribution can be determined from a single laboratory analysis using the rationale that the true value for A for any kerogen should fall in the middle of the symmetrical compensation ellipse (e.g., Lakshmanan et al. 1991; Nielsen and Dahl 1991; Nordeng 2015; Waples 2016). ORFA kinetic modeling considered only the S_2 fraction (Appendix D). ORFA kinetic modeling operates on a trial and error basis starting with a user-specified standard E_a distribution (specified as 41 to 72 E_a in this study) and then increases or decreases the amount at each E_a until the improvement in the fit falls below the pre-set limit. The process stops after a user-specified number of iterations (specified as 25 in this study). If the maximum allowed iterations are used, the user should increase the maximum number of iterations allowed and repeat until a satisfactory fit is reached prior to all specified iterations being used.

Palynological Analysis

About 5 g of each of the 13 samples was processed at the British Geological Survey using hydrochloric (36%) and hydrofluoric (40%) acid to remove all carbonates and silicates. *Lycopodium clavatum* (Batch No. 3862) was then added to the samples to enable concentration and flux calculations using the marker grain method (Stockmarr 1971; Maher 1981). The kerogen fraction was sieved using a 10- μm nylon mesh and was strew-mounted on microslides using Elvacite™. Sample SSK55335 had an unusual amount of mineral matter (presumably CaF_2) left after the standard palynological processing and the kerogen fraction was boiled in 36% HCl to remove the CaF_2 . A Nikon Eclipse Ci-L microscope equipped with a Prior H101A Motorized Stage (controlled by a Prior™ Proscan III unit connected to a PC with the open source software $\mu\text{manager}$; <http://micro-manager.org/wiki/Micro-Manager>) was used for optical examination of organic particles; routine study was conducted at 400 \times magnification while morphological details were analyzed at 1000 \times magnification. Following the palynofacies classification of Tyson (1995), 300 particles per sample were identified using randomly generated slide positions (Appendix A). In addition, each sample was studied using blue light excitation (near UV) on a Zeiss Universal microscope oper-

ating in incident-light mode with a III RS condenser set and the Zeiss filter set 09 (exciter filter: 450–490 nm; chromatic beam splitter: 510 nm; barrier filter: 515–565 nm) following the standard procedures for epifluorescence observations on palynological slides (Tyson 1995, 2006) (Table 2). Due to the relatively high palynomorph count in two slides (samples SSK55363 and SSK55999), these were also scanned for the presence of spores, which were recorded separately to palynofacies analysis (Appendix B). The kerogen isolate of sample SSK55999 was split, and one part was oxidized using 5 ml of fuming HNO_3 to allow detailed spore analysis.

RESULTS

Lithofacies Analysis

The studied Marl Hill succession contains a total of five fine-grained mud-rich lithofacies comprising calcareous claystone, calcareous mudstone, argillaceous mudstone, calcareous siltstone and calcareous sandy mudstone (Facies 1–5; Figs. 2 and 3; Newport et al. 2017). Summarized descriptions based on sedimentological logging and optical microscopy, and interpreted mode of deposition, for each facies are given in Figure 3.

Geochemical Analysis: Total Organic Carbon (TOC) and Rock-Eval

Organic matter (OM) richness within the study is highly variable (1.57 to 11.16 wt% TOC; Table 1). The highest TOC values are found in calcareous claystones which occur within, or adjacent to, the B_{2b} biozone (Figs. 2 and 3; Table 1). The lowest TOC value is present in the calcareous sandy mudstone, which occurs at the base of the B_{2b} biozone (Figs. 2 and 3; Table 1). A broad trend of decreasing organic matter richness with increasing grain size occurs (Fig. 4a; Table 1). All samples plot within kerogen Type II/III and III regions on a TOC vs. S_2 plot (Fig. 4a) but within Type I regions on a modified van Krevelen plot (Fig. 4b).

Eight Rock-Eval parameters (S_1 , S_2 , S_3 , HI_{pd} , OI_{pd} , T_{max} , PI and PY) and TOC_{pd} for the 13 samples are summarized in Table 1. In Figure 2, we show TOC_{pd} , T_{max} , S_1 , S_2 , HI_{pd} and OI_{pd} alongside the sedimentological log. The highest variabilities in TOC_{pd} and pyrolysate yield ($S_1 + S_2$) are observed

	Description	Interpretation
Facies 1: Calcareous Claystone	Mid grey to dark grey calcareous claystone, occurs in homogenous successions 0.001 < 1.3m contains planar lamination and discrete intervals with claystone intraclasts. Common ammonoid fossils and microfossils include foraminifera, radiolaria and spats (juvenile ammonoids).	Deposition from dilute waning density flows (fine grained turbidite, T_{E3} of Talling et al. 2012) due to evidence of traction. However, contribution from hemipelagic suspension settling may be significant.
Facies 2: Calcareous Mudstone	Pale to dark grey calcareous mudstone, occurs in normally graded beds 0.01 < 0.1 m thick contain planar lamination. Pyritic lags and lithoclasts of mudstone sometimes present at the base of beds. Clay-rich intraclasts are common throughout. Common indeterminate shell fragments occur in localised packages as well as disarticulated crinoid ossicles, fragmented bivalves, brachiopod and ammonoid fossils. Microfossils include foraminifera and sponge spicules.	Deposition from waning density flow (turbidite, T_{E1} , T_{E2} and T_{E3} of Talling et al. 2012) due to normally graded beds, presence of claystone intraclasts, mudstone lithoclasts and fragmented shell material. However, a significant contribution of sediment from hemipelagic suspension settling cannot be entirely ruled out.
Facies 3: Argillaceous Mudstone	Mid grey argillaceous mudstone, occurs in massive or normally graded beds 0.1 < 1.5 m thick contain planar lamination. Clay-rich intraclasts are very common throughout the facies. Rare indeterminate fragmented shell material and fragmented ammonoid fossils, common microfossils include foraminifera.	Deposition from waning density flow (turbidite, T_{E1} , T_{E2} and T_{E3} of Talling et al. 2012) due to normally graded beds, presence of claystone intraclasts, mudstone lithoclasts and fragmented shell material. The greater proportion of argillaceous sediment suggest the source of the sediment was more argillaceous and less carbonate rich compared to Facies 2.
	Description	Interpretation
Facies 4: Calcareous Siltstone	Pale to mid grey calcareous siltstone, occurs in normally graded beds 0.01 < 0.4 m thick contain sharp or erosive bases, shell lags, ripple cross-lamination and convolute lamination. Common indeterminate fragments of shell material including disarticulated crinoid ossicles, fragmented bivalves and corals. Microfossils include foraminifera and sponge spicules.	Deposition from waning density flow (turbidite, T_D and T_{E1} of Talling et al. 2012) due to normally graded beds with erosive bases. The larger grainsize relative to Facies 2 and 3 as well as the presence of ripple cross lamination indicates deposition from higher energy flows.
Facies 5: Calcareous sandy Mudstone	Pale to mid-grey sandy mudstone, occurs in highly disturbed beds 0.05 < 0.5 m thick containing weak normal or reverse grading, dispersed mudstone lithoclasts and significant detrital and bioclastic carbonate material. Bioturbation is common throughout (BI = 2 < 4). Shell fragments include rugose corals, crinoid ossicles, bivalves, brachiopods and ammonoids. Microfossils include foraminifera, radiolaria and sponge spicules.	Deposition from low strength cohesive debrites (D_{M1} of Talling et al. 2012) due to weak normal and inverse grading, the abundance of scattered lithoclasts and carbonate allochems supported by a claystone matrix.

Figure 3. Summary table of the five lithofacies identified within the Marl Hill borehole (MHD 11).

Table 1. Present-day TOC and Rock–Eval primary and secondary parameters (S_1 , S_2 , S_3 , T_{\max} and HI and OI)

Sample (SSK) number	Lithofacies	Organofacies	Total organic carbon (TOC _{pd}) (wt%)	S_1 (mg/g)	S_2 (mg/g)	S_3 (mg/g)	Hydrogen index, HI _{pd} (mg HC/g TOC _{pd})	Oxygen Index, OI _{pd} (mg CO ₂ /g TOC _{pd})	T_{\max} (°C)	Production index, PI	Pyrosylate yield, PY
55296	Argillaceous mudstone	Intermediate	3.81	1.24	8.99	0.73	236	19	434	0.12	10.23
55308	Argillaceous mudstone	B	3.79	0.71	5.53	0.33	146	9	435	0.11	6.24
55320	Calcareous mudstone	A	5.46	1.36	18.25	0.36	334	7	438	0.07	19.61
55323	Calcareous mudstone	A	4.71	0.97	11.87	0.26	252	6	439	0.08	12.84
55326	Calcareous mudstone	A	5.31	1.43	14.84	0.30	280	6	440	0.09	16.27
55335	Calcareous mudstone	Intermediate	5.50	1.70	17.13	0.41	311	7	439	0.09	18.83
55351	Calcareous siltstone	A	3.78	0.83	7.81	0.36	206	10	437	0.10	8.64
55363	Calcareous siltstone	B	3.70	0.73	4.88	0.36	132	10	441	0.13	5.61
55365	Calcareous mudstone	Intermediate	5.09	0.95	9.02	0.39	177	8	437	0.10	9.97
55366	Calcareous claystone	A	11.16	2.26	30.34	0.37	272	3	441	0.07	32.60
55999	Calcareous sandy mudstone	B	1.57	0.21	1.41	0.20	90	13	442	0.13	1.62
56000	Calcareous claystone	A	9.55	1.57	18.40	0.26	193	3	440	0.08	19.97
56001	Calcareous claystone	Intermediate	3.97	0.79	6.84	0.26	172	7	442	0.10	7.63

within, and adjacent to, the B_{2b} biozone (Table 1; Fig. 2). The P₂ and E_{1a} biozones, in contrast, appear to show less variability in organic geochemistry particularly relating to TOC_{pd} (Fig. 2). All oxygen index (OI_{pd}) values are relatively low (3 to 19 mg/g), indicating that all samples have undergone limited oxidation suggesting high levels of OM preservation (Table 1). All samples analyzed are within the early oil window as indicated by the T_{\max} range of 434 °C to 442 °C and production index values of 0.07 to 0.13 (Table 1; Figs. 2 and 4b).

Kerogen Kinetic Analysis: One-Run-Fixed-Arrhenius (ORFA)

All samples analyzed using a fixed A value of $2 \times 10^{14} \text{ s}^{-1}$ contain relatively narrow activation energy (E_a) distributions, with the majority of E_a

abundance occurring between 53 and 59 kcal/mol (Fig. 5; Appendix C). However, significant variation occurs at the 56 kcal/mol peak (Fig. 6). Three different organofacies were determined based on the abundance of this activation energy peak with two end members identified: an absence (or < 5%) indicating ‘organofacies A’ (Fig. 5a); a presence (> 15%) indicating ‘organofacies B’ (Fig. 5b); and an intermediate presence (5 to 15%) indicating a mixed or ‘intermediate organofacies’ (Fig. 5c).

Organofacies A samples ($N = 6$) consist mainly of calcareous mudstones and calcareous claystones; contain the highest organic matter richness (3.78–11.16; average 6.67 wt%); have high pyrolysate yield (8.64–32.60; average 18.32); have low production indices (0.07–0.10; average 0.08); have relatively high hydrogen indices (193–334; average 256); and contain mainly Type II/III kerogen on a TOC vs. S_2 plot (Figs. 3 and 4a; Table 1).

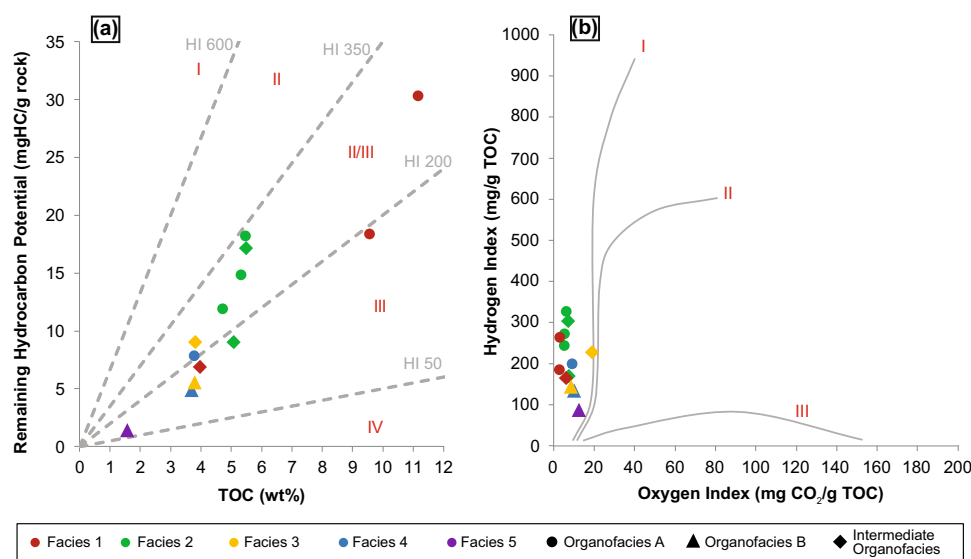


Figure 4. (a) (left): Kerogen quality plot indicating the kerogen type of the remaining total organic matter (y -axis corresponds to the S_2 from Rock-Eval). The majority of samples plot as Type II/III or III. (b) (right): modified van Krevelen plot indicating the majority of samples are Type I.

Organofacies B samples ($N = 3$) consist of argillaceous mudstones, calcareous siltstones and calcareous sandy mudstones; contain the lowest organic matter richness (1.57 to 3.79; average 3.01 wt%); have relatively low pyrolysate yield (1.62 to 6.24; average 4.49); have relatively high production indices (0.11 to 0.13; average 0.12); have low hydrogen indices (90 to 146; average 123); and contain predominantly Type III kerogen on a TOC vs. S_2 plot (Figs. 3 and 4a; Table 1).

Intermediate organofacies samples ($N = 4$) consist of argillaceous mudstones, calcareous mudstones and calcareous claystones; contain good organic matter richness (3.81 to 5.50; average 4.59 wt%); have moderate pyrolysate yield (9.97 to 19.97; average 14.75); have intermediate production indices (0.09 to 0.12; average 0.10); have relatively high hydrogen indices (172 to 311; average 224); and contain both Type II/III and Type III kerogen on a TOC vs. S_2 plot (Figs. 3 and 4a; Table 1).

Palynofacies Analysis

Palynofacies assessment of 13 samples followed the procedure proposed by Tyson (1995) wherein structureless (heterogeneous and homogeneous) amorphous organic matter (AOM) is distinguished from structured material (phytoclasts, sporomorphs,

phytoplankton, fungal remains) and any residual mineral matter, typically pyrite, which was not removed during sample preparation (Appendix A). The palynofacies analysis is summarized using an AOM–Phytoclast–Palynomorph (APP) triplot (Fig. 7; after Tyson 1995). The spore counts of SSK55363 and SSK55999 are summarized in Appendix B.

Amorphous Organic Matter

Structureless organic (AOM) constituents dominate the kerogen fractions with an average 81% of the counts with a minimum of 34% (SSK55363; 60.1 m) and a maximum of 96% (SSK55351; 46.25 m). Within this structureless category, heterogeneous AOM is dominant comprising an average of 50% of the total counts (minimum of 23%—SSK55363, 60.1 m; maximum of 83%—SSK55335, 31.6 m), with pellicular AOM the most important constituent of all heterogeneous AOM. Homogenous AOM comprises an average of 34% of the total counts (minimum of 11%—SSK55363, 60.1 m; maximum of 69%—SSK55351, 46.2 m), with the most important constituent of all homogenous AOM being grumose AOM with a gelified matrix.

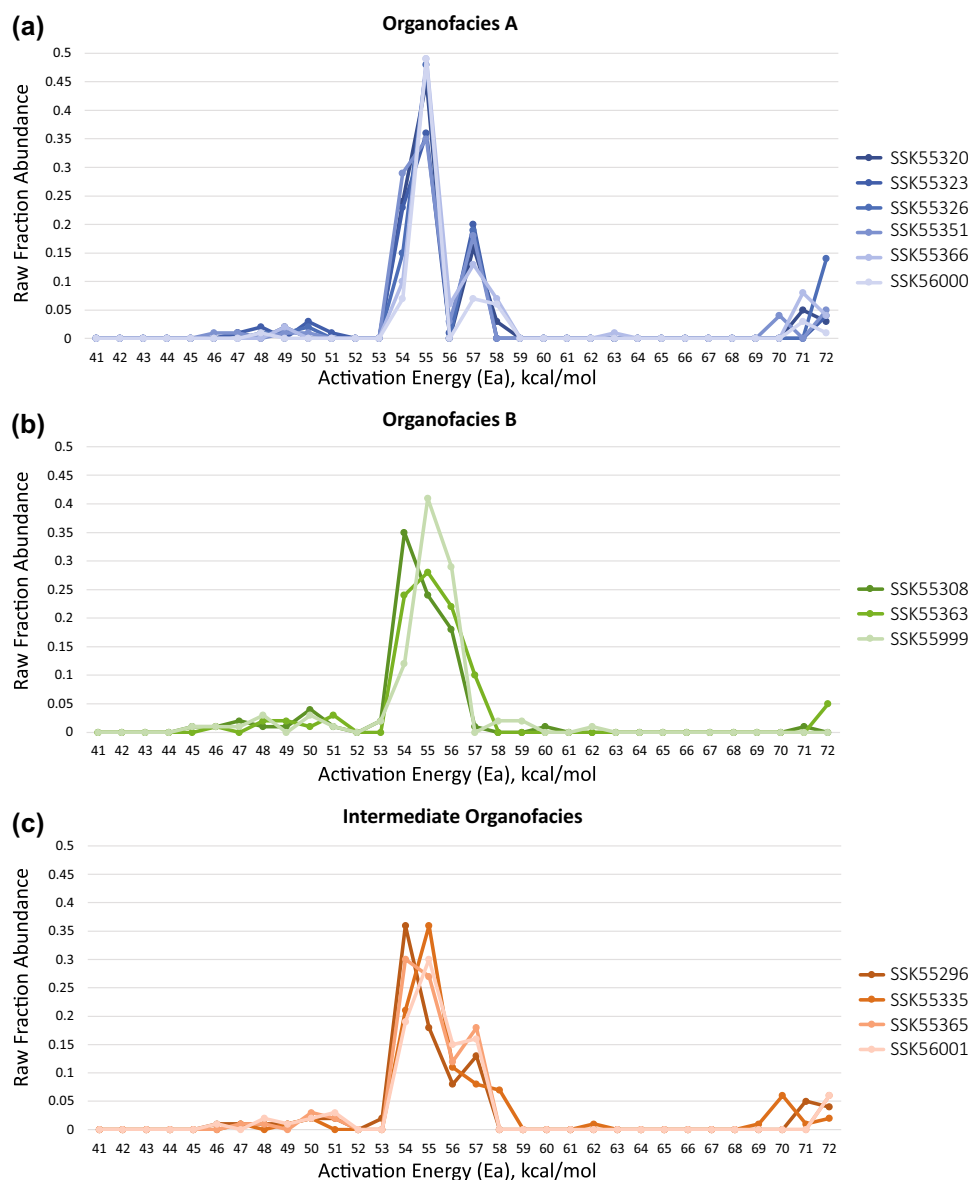


Figure 5. Activation energy distribution as raw fraction abundance for all samples: (top) organofacies A, (middle) organofacies B and (bottom) intermediate organofacies. The greatest variation in activation energy distribution occurs at the 56 kcal/mol peak: organofacies A samples contain < 5%; organofacies B samples contain > 15%; intermediate organofacies contain between 5 and 15% peak abundance.

Structured Organic Matter

Of the structured organic material phytoclasts are the most abundant (average 11%; minimum 2%—SSK55335, 31.6 m; maximum 28%—SSK55363, 60.1 m). Phytoclasts are most abundant within, and adjacent to, the B_{2b} biozone (Fig. 2; Appendix A). Algal components are very rare but are present in 3 samples with relatively low abundance (average 0.2%; where present minimum

of 0.34%—SSK55320, 20.9 m and SSK55365, 62 m; maximum of 1.67%—SSK55366, 62.8 m). Paly-nomorphs occur within all samples and represent an average 7% of the total counts (minimum < 1%—SSK55351, 46.25 m; maximum 38%—SSK55363, 60.1 m). Sporomorphs are by far the most dominant palynomorph Type present with the most common species consisting of *Lycospora pusilla*, *Lycospora spp.* and *Densosporites anulatus* (Appendix A).

Organofacies A

Organofacies A samples ($N = 6$) show structureless organic (AOM) constituents dominate the kerogen fraction with an average of 89% of the counts with a minimum of 83% (SSK56000, 64.3 m) and a maximum of 96% (SSK55351, 46.2 m). Within this structureless category, heterogeneous AOM is dominant comprising an average of 51% of the total counts (minimum of 29%—SSK56000, 64.3 m; maximum of 68%—SSK55366, 62.8 m), with the most important constituent being pellicular AOM following the overall trend throughout the samples. Homogenous AOM comprises an average of 38% of total counts (minimum of 16%—SSK55323, 23.4 m; maximum of 69%—SSK55351, 46.2 m), grumose AOM with a gelified matrix is the most important constituent of all homogenous AOM. Structured organic matter accounts for an average of only 11% of total counts, with phytoclasts being the most abundant (average 6%; minimum 4%—SSK55351, 46.2 m; maximum 9%—SSK56000, 65.1 m). Palynomorphs, on average, account for < 4% of total counts (minimum < 1%—SSK55351, 46.2 m; maximum 8%—SSK56000, 65.1 m), with sporomorphs contributing the majority of counts. Algal components are present, albeit in low abundance, in two of the six samples identified as organofacies A (SSK55320, 20.9 m and SSK55366, 62.8 m; Appendix A and Fig. 2).

Organofacies B

Organofacies B samples ($N = 3$) show structureless organic (AOM) constituents as the largest proportion of the kerogen fraction with an average of 59% of the counts with a minimum of 34% (SSK55363, 60.1 m) and a maximum of 82% (SSK55308, 15.6 m). Within this structureless category, heterogeneous AOM is more dominant comprising an average of 34% of the total counts (minimum of 23%—SSK55363, 60.1 m; maximum of 40%—SSK55308, 15.6 m and SSK55366, 62.8 m), with the most important constituent being pellicular AOM following the overall trend throughout the samples. Homogeneous AOM comprises an average of 25% of total counts (minimum of 11%—SSK55363, 60.1 m; maximum of 42%—SSK55308, 15.6 m), grumose AOM with a gelified matrix is the most important constituent of all homogenous AOM. Structured organic matter accounts for an average of

41% of total counts, with both phytoclasts (average 19%; minimum 7%—SSK55308, 15.6 m; maximum 28%—SSK55363, 60.1 m) and sporomorphs (average 18%; minimum 6%—SSK55308, 15.6 m; maximum 37%—SSK55363, 60.1 m) contributing the majority of counts. No algal components are present in the three samples identified as organofacies B (Appendix A and Fig. 2).

Intermediate Organofacies

Intermediate organofacies samples ($N = 4$) show structureless organic (AOM) constituents dominate the kerogen fraction with an average of 86% of the counts with a minimum of 78% (SSK55365, 62.0 m) and a maximum of 94% (SSK55335, 31.6 m). Within this structureless category, heterogeneous AOM is dominant comprising an average of 59% of the total counts (minimum of 36%—SSK56001, 65.1 m; maximum of 83%—SSK55335, 31.6 m), with the most important constituent being pellicular AOM following the overall trend throughout the samples. Homogenous AOM comprises an average of 26% of total counts (minimum of 11%—SSK55335, 31.6 m; maximum of 44%—SSK56001, 65.1 m), of all homogenous AOM, grumose AOM with a gelified matrix is the most important constituent. Structured organic matter accounts for an average of 14% of total counts, with phytoclasts being the most abundant (average 9%; minimum 2%—SSK55335, 31.6 m; maximum 16%—SSK55365, 62.0 m). Palynomorphs, on average, account for < 3% of total counts (minimum < 2%—SSK55296, 6.2 m; maximum < 4%—SSK56001, 65.1 m), with sporomorphs contributing the majority of counts. Algal components are present in low abundance in one sample identified as intermediate organofacies (SSK55365, 62.0 m; Appendix A and Fig. 2).

DISCUSSION

Using organofacies defined from kerogen kinetic data (A, B and Intermediate; Fig. 5) direct comparisons of organic geochemical, sedimentological and palynological datasets were made. These have been grouped into observations linked to organic matter quantity and quality, determination of depositional environment and prospectivity of the Bowland Shale Formation.

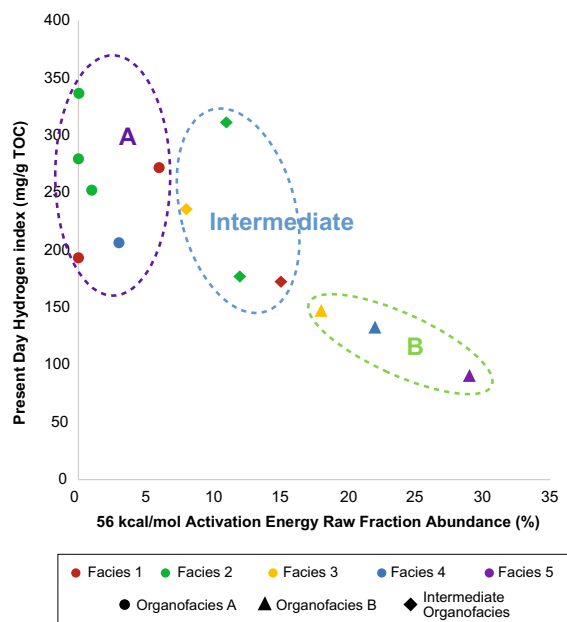


Figure 6. Relationship between present day hydrogen index values and concentration of organic matter with an activation energy of 56 kcal/mol. Three distinct organofacies can be observed as indicated by dashed lines.

Organic Matter Quantity and Quality

The assessment of source potential for any given system requires various parameters to be determined: the quantity of OM (i.e., TOC present in the source rock); the quality of OM (the proportions of individual kerogens and the prevalence of long-chain hydrocarbons) and the thermal maturity of the source rock (i.e., pyrolysis T_{max}). Various authors have proposed specific criteria, based on these parameters, which must be fulfilled in order for a source rock to be prospective as a shale-gas play: > 2 wt% TOC at present day (Gilman and Robinson 2011; Andrews 2013); Type II (Jarvie 2012) or a mixture of Types I, II and IIS (Charpentier and Cook 2011); original hydrogen index (HI_o) values > 250 mg/g (Charpentier and Cook 2011) and 250 to 800 mg/g (Jarvie 2012); and thermal maturity between 1.1 and 3.5% R_o (i.e., within the gas window; Jarvie 2012).

Kerogen typing from palynological analysis within this study follows the genetic system proposed by Tyson (1995) wherein Type I consists of algal material; Type II consists of spores and pollen, phytoplankton and cuticles; Type III consists of homogenous AOM and phytoclasts; and Type IV

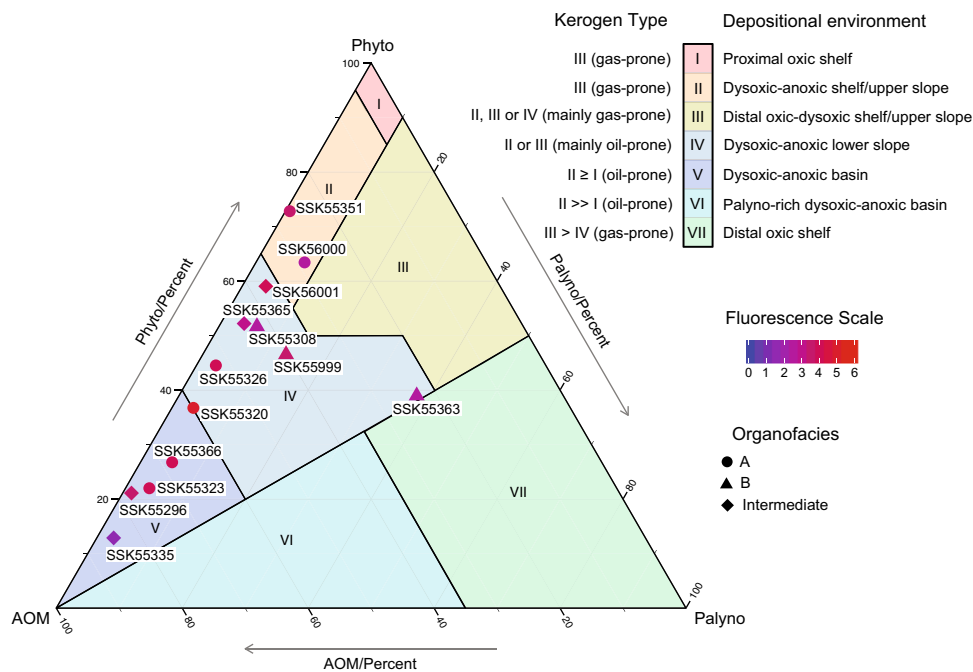


Figure 7. Ternary Amorphous Organic Matter (AOM)—Phytoclast (Phyto)—Palynomorph (Palyno) plot for the samples from the Marl Hill (MHD 11) core. (Modified after Tyson 1995).

Table 2. Calculated original TOC_o and HI_o based on the calculated kerogen typing using a combination of palynofacies analysis and the fluorescence scale

Sample (SSK) number	Lithofacies	Organofacies	Total organic carbon (TOC_o) (wt%)	Hydrogen index, HI_o (mg HC/g TOC_{pd})	FS	FSI	Type I	Type II	Type III	Type IV
55296	Argillaceous mudstone	Intermediate	4.39	493	3.5	3.39	42.2	33.8	20.0	0.0
55308	Argillaceous mudstone	B	4.08	310	2.5	2.30	15.4	30.3	48.7	0.0
55320	Calcareous mudstone	A	5.62	459	5	4.73	46.6	15.1	35.0	0.0
55323	Calcareous mudstone	A	5.62	505	4	3.79	45.4	30.9	20.7	0.0
55326	Calcareous mudstone	A	5.41	391	4	3.76	31.9	22.4	42.0	0.0
55335	Calcareous mudstone	Intermediate	5.71	442	1.5	1.46	20.2	65.4	13.0	0.0
55351	Calcareous siltstone	A	3.63	253	3.5	3.37	14.8	12.2	72.3	0.0
55363	Calcareous siltstone	B	4.13	334	2.5	1.36	5.2	55.1	38.7	0.0
55365	Calcareous mudstone	Intermediate	5.51	327	3	2.48	18.3	28.7	51.0	0.0
55366	Calcareous claystone	A	13.64	487	4	3.76	44.3	27.4	26.3	0.0
55999	Calcareous sandy mudstone	B	1.63	339	3.5	2.55	16.8	35.2	45.0	0.0
56000	Calcareous claystone	A	9.92	271	2.5	2.25	10.8	25.6	63.0	0.0
56001	Calcareous claystone	Intermediate	4.18	312	4	3.40	20.6	19.7	57.3	0.0

consists of coalified material (Table 3). The empirical system defined only by the range of HI and OI (or H/C and O/C; Table 3) is often used in combination with Rock-Eval data, as shown on the modified van Krevelen plot (Fig. 4b). As all samples within the study come from the same borehole (MHD 11) with a reasonably narrow stratigraphic range (5 m to 65 m) the variation in thermal maturity is negligible. All samples, regardless of organofacies, are within the early oil window as indicated by the T_{max} range of 434 °C to 442 °C and production index values of 0.07 to 0.13 (Table 1; Figs. 2 and 4b).

Fluorescence, HI_o and TOC_o

It is important to note that a proportion of the heterogeneous AOM could represent degraded algal material and therefore signify Type I kerogen

(Hennissen et al. 2017). In order to determine whether this is applicable to any of the heterogeneous AOM measured within the study a technique known as fluorescence scale (FS) was utilized (Tyson 2006). The technique works on the premise that fluorophores (such as carotenoids of sporinite, isoprenoids of alginite and the phenols of cutinite and suberinite) result in samples rich in heterogeneous AOM generally exhibiting a stronger fluorescence; their fluorescence is further enhanced when these compounds are distributed in an aliphatic environment (Robert 1988; Lin and Davis 1988; Tyson 2006). The fluorescence scale index (FSI) can be calculated from the fluorescence scale (FS) and the relative abundances of amorphous organic matter (AOM) and phytoclasts (Phyto; Eq. 2; Appendix A and Table 3).

$$FSI = FS \times \left(\frac{AOM}{AOM + Phyto} \right) \quad (2)$$

The maximum value for FSI (and FS) is 6 where the palynological counts reach 100% AOM. In order to determine an estimate of the abundance of highly fluorescent algal material (potentially Type I kerogen) within the sample, it is necessary to divide the FSI by 6 and multiply it with the relative abundance of heterogeneous AOM. The remainder of the fraction of heterogeneous AOM is then regarded as Type II kerogen (Hennissen et al. 2017).

Once the relative proportions of kerogen types have been established using visual kerogen assessment (i.e., palynological study), it is then possible to use the HI_o equation of Jarvie et al. (2007):

$$HI_o = \left(\frac{\%TypeI}{100} \times 750 \right) + \left(\frac{\%TypeII}{100} \times 450 \right) + \left(\frac{\%TypeIII}{100} \times 125 \right) + \left(\frac{\%TypeIV}{100} \times 50 \right) \quad (3)$$

It is important to note that the weighting factors for kerogen type used within Eq. 3 are derived from

pyrolysis data of pure Type I, II, III and IV kerogen from the Barnett Shale (Jarvie et al. 2007). This technique is currently the best approach, but greater accuracy could be achieved if weighting factors specific to the Bowland Shale were available. After HI_o has been determined, TOC_o can also be deduced using the equation of Jarvie (2012):

$$TOC_o = \frac{[TOC_{pd}(0.085 \times (S1_{pd} + S2_{pd}))] - (HI_o \times 0.0008)}{(1 - HI_o/1177)}$$

The HI_o and TOC_o results for all samples are summarized in Table 2.

Organofacies A

Organofacies A samples (< 5% or absent $56 E_a$ peak) contain the highest organic matter richness, hydrogen indices and pyrolysate yields, and consist predominantly of Type II/III kerogen (TOC vs. S_2 plot; but Type I kerogen on a modified van Krevelen

Table 3. Comparison between elemental and visual characterization of kerogen type

Kerogen type	Elemental (or Rock-Eval derived) After van Krevelen (1961), Durand and Espitalié (1973), Espitalié et al. (1977), Tissot et al. (1974), Durand and Monin (1980), Tissot and Welte (1984), Vandenbroucke and Largeau (2007)	Visual After Tyson (1995), Hennissen et al. (2017)
Type I	High initial H/C ratios > 1.5 and low initial O/C ratios between 0.03 to 0.1 Lipid-rich organic matter, derived either from algal or cyanobacterial materials (e.g., botryococcus) or from biodegradation (microbial lipids) Chemical composition typically dominated by saturated aliphatic (acyclic) compounds and an abundance of normal and branched alkane hydrocarbons (paraffins) High potential to hydrocarbon generation	Very strongly fluorescent OM including: Algal material (marine and freshwater) Amorphous material (derived from cyanobacteria and thiobacteria)
Type II	Relatively high H/C ratios between 1.0 < 1.3 and low O/C ratios (~ 0.15) Typically derived from pollen grains, spores, cuticles and marine planktonic biomass, i.e., phytoplankton, zooplankton, microorganisms (bacteria) deposited under oxygen depleted conditions Chemical composition typically contains more polyaromatic nuclei and heteroatomic functional groups than Type I, but less than Type III High potential to hydrocarbon generation	Fluorescent (non-oxidized) OM including: Amorphous OM (AOM; derived from phytoplankton) Non-alginitic palynomorphs (spores or pollen) Cuticles Membranous debris
Type III	Relatively low initial H/C ratios usually < 1 and relatively high initial O/C ratio < 0.3 Typically derived from terrestrial higher plants, often highly reworked and contain recognizable debris of evolved plants and vitrinite splinters Chemical composition is dominated by polycyclical aromatic hydrocarbons and oxygenated functional groups, but microbial degradation may contribute a paraffinic component Oil potential is moderate, although at greater depths, gas potential is high	Non-fluorescent OM including: Homogenous AOM (translucent, structureless) Phytoclasts (translucent, structured) Woody fragments Palynomorphs (partially oxidized) Plankton-derived material (partially derived)
Type IV	Abnormally low H/C ratios < 0.8 and relatively high O/C ratios 0.2 > 0.3 Typically derived from the biodegradation, oxidation or from thermal degradation of organic matter Often referred to as 'residual' or 'inert' material No potential to hydrocarbon generation	Non-fluorescent (generally oxidized or carbonized or 'coalified material') OM: Phytoclasts (including charcoal) Fungal and chitinous materials

plot) based on TOC and Rock–Eval data (Table 1; Figs. 3 and 4). The variation in kerogen typing based on Rock–Eval plots is a result of low OI (average 5.83 mg/g; minimum of 3 mg/g—calcareous claystone: SSK55366, 62.8 m and SSK56000, 64.3 m; maximum of 10 mg/g—calcareous siltstone: SSK55351, 46.2 m) ensuring samples place in the Type I region within a modified van Krevelen (Fig. 4b); but high TOC: S_2 ratios result in samples plotting within Type II/III region of the TOC vs. S_2 plot (Fig. 4a). If the modified van Krevelen shows the correct kerogen typing (Type I), then the lower than expected HI values from whole rock pyrolysis could be a result of woody phytoclasts partially oxidizing; or a reduced signal from the small volume of spores, pollen and non-prasinophyte acritarchs present within the sample; or from partially degraded planktonic or bacterial amorphous kerogen with little or no vitrinite (Tyson 1995). Low OI values, < 20 mg/g, indicate limited oxidation has occurred (Table 1) suggesting that significant degradation of organic matter is unlikely to have occurred. However, palynological data show that organofacies A samples contain the highest amount of structureless organic matter (AOM; average of 89% of the total counts) with a significant contribution from heterogeneous AOM (average of 51% of the total counts). The structureless organic matter represents degraded OM in some way, shape or form; most likely algal material (including acritarchs). Very few acritarchs are recovered in this study and indeed throughout the Carboniferous as it falls within an approximately 100 Myr interval known as the ‘Late Paleozoic phytoplankton black-out’ lasting from the Mississippian to the early Triassic when very few phytoplanktonic organisms are reported in the fossil record (Riegel 2008). Because there is no proof of a breakdown of the trophic web, proven by the abundance of benthic organisms during the same period, the most plausible explanation is a reduction in the abundance of cyst forming phytoplankton due to an abundant nutrient supply; a combined effect from tectonic activity during the formation of Pangaea and glacial erosion in the southern hemisphere (Servais et al. 2016). Structured organic matter within the organofacies consists of an average of only 11% of the total counts, of which phytoclasts are the most dominant component (average of < 6%), followed by sporomorphs (average of < 4%; Fig. 7). Algal components are present, albeit in low abundance, in two of

the six samples (SSK55320, 20.9 m and SSK55366, 62.8 m; Appendix A and Fig. 2).

Organofacies A samples, when corrected using the FSI and Eq. 2, show a significant portion of potential Type I kerogen (average of 32%; minimum of 10.8%—SSK56000, 64.4 m; maximum of 46.6%—SSK55320, 20.9 m; Table 2) correlating with the empirical typing from the modified van Krevelen plot (Fig. 4b). Type II kerogen (average of 22%; minimum of 12.2%—SSK55351, 46.2 m; maximum of 30.9%, SSK55323, 23.4 m) and Type III kerogen (average of 43.2%; minimum of 20.7%—SSK55323, 23.4 m; maximum of 72.3%—SSK55351, 46.2 m) comprise the remaining kerogen within the organofacies (Table 2). Therefore, organofacies A contains a significant portion of Type I kerogens (algal components), which was not shown on the TOC vs. S_2 (Fig. 4a) but is indicated by the palynological analysis, modified van Krevelen plot and from the distribution of activation energies (Appendix A and Table 3; Figs. 4b, 5 and 7).

Organofacies A samples average HI_o (394; minimum of 253—SSK55351, 46.2 m; maximum of 505—SSK55323, 23.4 m) and average TOC_o (7.31 wt%; minimum of 3.63 wt%—SSK55351, 46.2 m; maximum of 13.64 wt%—SSK55366, 62.8 m) fall comfortably within the criteria previously discussed for a prospective shale-gas play, although samples are not thermally mature. It is interesting to note the similarities in % AOM; FS; % phytoclasts; HI; kerogen type and TOC% between organofacies A described in this study with the marine organic facies AB of Tyson (1995) and organic facies B/C of Evenick and McCain (2013).

Organofacies B

Organofacies B samples (> 15% abundance of 56 E_a peak) contain the lowest organic matter richness, hydrogen indices and pyrolysate yields, and consist principally of Type III kerogen (TOC vs. S_2 plot; but Type I kerogen on a modified van Krevelen plot) based on TOC and Rock–Eval data (Table 1; Figs. 3 and 4). The variation in kerogen typing based on Rock–Eval plots is likely to occur due to the reasons previously discussed for organofacies A. Palynological data show that organofacies B samples, similar to organofacies A, contain structureless organic matter as the largest overall proportion (AOM; average of 59%; heterogeneous AOM

comprising 34% and homogenous AOM comprising 25% of total counts; Fig. 7). It is important to note that while AOM is still the dominant type of OM the relative proportion is significantly reduced when compared to organofacies A (average of 89%; heterogeneous AOM comprising 51% and homogenous AOM comprising of 38% of total counts). Structured organic matter within organofacies B consists of an average of 41% of total counts, with both phytoclasts (average of 19%) and sporomorphs (average of 18%) contributing the majority of total counts; indicating that organofacies B has a higher terrestrial influence (Appendix A). Relative to organofacies A, organofacies B contains 30% more structured organic matter with the most significant increase attributed to sporomorphs (Fig. 7). No algal components were directly observed in the three samples identified as organofacies B (Appendix A and Fig. 2). However, when corrected using FSI and Eq. 2, organofacies B do contain potential Type I kerogens (average of 12.5%; minimum of 5.2%—SSK55363, 60.1 m; maximum of 16.8%—SSK55999, 63.7 m; Table 2). Type II kerogen (average of 40.2%; minimum of 30.3%—SSK55308, 15.6 m; maximum of 55.1%—SSK55363, 60.1 m) and Type III kerogen (average of 44.1%; minimum of 38.7%—SSK55363; maximum of 48.7%—SSK55308, 15.6 m) comprise the remaining kerogen within the organofacies (Table 2).

In contrast to organofacies A, organofacies B contains significantly more Type II and III kerogen which correlates with the palynological data that shows a significant increase in sporomorphs and phytoclasts relative to organofacies A. Similar to organofacies A, organofacies B does contain a proportion of Type I kerogen which was shown on the modified van Krevelen diagram (Fig. 4b) but palynological analysis reveals that Type III kerogen is the most dominant kerogen type present (Appendix A and Table 3).

Organofacies B samples average HI_o (327; minimum of 310—SSK55308, 15.6 m; maximum of 339—SSK55999, 63.7 m) and average TOC_o (3.28 wt%; minimum of 1.63 wt%—SSK5599, 63.7 m; maximum of 4.13 wt%—SSK55363, 60.1 m) also fall within the criteria previously discussed for a prospective shale-gas play, thus meaning regardless of organofacies all samples are prospective as source rock reservoirs when sufficiently thermally mature. It is interesting to note the similarities in % AOM; FS; % phytoclasts; HI; kerogen type and TOC_o

between organofacies B described in this study with the marine organic facies BC of Tyson (1995) and organic facies B/E of Evenick and McCain (2013).

Intermediate Organofacies

In addition to the two-end-member organofacies, a mixed or 'intermediate organofacies' with a 5 to 15% abundance (Fig. 5c) occurs, these samples contain mixed characteristics of both organofacies A and B on a sliding scale with some samples closely resembling organofacies A (e.g., SSK55296: 92% AOM and 5% structured OM; 42.2% Type I kerogen) while other closely resemble organofacies B (e.g., SSK55365: 78% AOM and 15% structured OM; 18.3% Type I kerogen; Fig. 7). The wide spectrum of kerogen types present within intermediate organofacies, in combination with the distribution of activation energies, supports the conclusion that this organofacies is a result of mixing and dilution between the two-end-member facies.

Use of ORFA in Determining OM Quantity and Quality

The three different organofacies determined based on the abundance of the 56 kcal/mol activation energy peak consist of two-end-member organofacies: an absence (or < 5%) indicating 'organofacies A' (Fig. 5a) which contains the highest proportion of algal material and therefore Type I kerogen; and a presence (> 15%) indicating 'organofacies B' (Fig. 5b) which contains the highest proportion of sporomorphs and therefore Type II kerogen (Fig. 6, Appendix A and Table 3), thus demonstrating that the organofacies defined by the distribution of activation energies derived from One-Run-Fixed-Arrhenius kerogen kinetic analysis can establish and quantify a net effect in characterizing the organic matter quantity and quality. This is significant as ORFA data are less labor intensive than palynological studies and can be collected using existing Rock-Eval time, temperature and yield data; enabling cheaper and faster organic characterization to be available to geoscientists during source rock appraisal. However, caution must be exercised in drawing interpretations as to influences resulting in this effect such as biological source(s), organic matter mixing, preservation state(s) and

maturity without additional investigation using data derived from detailed palynological analysis.

Determination of Depositional Environment

The concept of a classification of sediments based on their organic matter characteristics emphasizes that it is the sedimentary and diagenetic environment that determines the initial kerogen composition (i.e., Jones and Demaison 1982). Extrapolation of this facies concept allows prediction of the probable initial organic facies properties (i.e., TOC, H/C, HI and likely OM source; e.g., Jones and Demaison 1982; Jones 1987; Tribovillard and Gorin 1991; Pepper and Corvi 1995; Tyson 1995; Evenick and McCain 2013). The AOM–Phytoclast–Palynomorph plot of Tyson (1995) used to determine approximate depositional environment based on the proportions of the three main kerogen groups has been modified to accommodate for the prior knowledge of the sedimentology of the succession (a mud-dominated lower slope succession with reduced sediment supply as sediments remained trapped on the largely flooded shelf; Newport et al. 2017).

Organofacies A plot in a continuum with intermediate organofacies between AOM and phytoclasts (Fig. 7). According to the APP plot, this places the depositional environment for these organofacies between dysoxic-anoxic shelf edge/upper slope; dysoxic-anoxic lower slope; and dysoxic-anoxic basin (Fig. 7). Organofacies A and intermediate organofacies samples consist of calcareous claystones, calcareous mudstones and argillaceous mudstones interpreted to represent deposition from dilute waning density flows (fine-grained turbidite; TE-1 to TE-3 of Talling et al. 2012) and background hemipelagic suspension settling (Fig. 3; Newport et al. 2017). Within these lithofacies, mud-rich intra-clasts (the product of erosion, transport and deposition of soft water-rich mud clasts; Schieber et al. 2010; Schieber 2016) have been observed (Newport et al. 2017); this has the implication that OM within sediments containing intra-clasts may contain OM from more than one source and could therefore explain the variation noted in kerogen type and interpreted depositional environment from the APP plot (Fig. 7; Table 2).

Organofacies B, in contrast, plot with increasing degree of enrichment in palynomorphs (Fig. 7). According to the APP plot, this places the depositional environment for organofacies B within a

dysoxic-anoxic lower slope (Fig. 7). Organofacies B samples consist of argillaceous mudstones, calcareous siltstones and calcareous sandy mudstones interpreted to represent deposition from dilute waning density flows (fine-grained turbidite; TE-1 to TD of Talling et al. 2012) and deposition from low-strength cohesive debrites (DM-1 of Talling et al. 2012; Fig. 3; Table 1; Newport et al. 2017). Higher sporomorph abundance typically occurs close to emergent land masses (i.e., the source) and it is not necessarily be expected within a lower slope setting. However, sediment transport mechanisms (i.e., turbidity currents and debris flows) enable bypass of the shelf edge and upper slope resulting in the transport of sporomorph-rich sediment to the lower slope. As all sediments which contain organofacies B were likely derived from density flows that traversed the shelf, or via density flows initiated on the upper slope; it provides an explanation as to how organofacies B samples within the slope succession at Marl Hill became relatively enriched in palynomorphs (in particular sporomorphs), thus providing the likely source of the OM.

With only ORFA data, accurate deduction of depositional environment would not be possible; however, when used in combination with organic petrographic techniques such as palynology, it becomes a valuable tool in highlighting any varying trends that may be present.

Prospectivity of the Bowland Shale Based on this Study

The Mississippian (326–332 Ma) mudstones, Bowland Shale Formation, deposited in the Bowland Basin are active unconventional exploration targets (Andrews 2013; Clarke et al. 2018). Previous studies have shown deposition primarily occurred via turbidites and debrites (Gawthorpe 1986, 1987; Newport et al. 2017). Five lithofacies have been identified with a coarse trend of decreasing organic matter richness (TOC_{pd}) with increased grain size (Newport et al. 2017). This study incorporates both organic geochemical (TOC, Rock-Eval and ORFA kerogen kinetic) and organic petrographic (palynofacies) analyses combined to provide a detailed assessment of the organofacies present.

The most dominant organofacies within the studied interval, organofacies A and intermediate organofacies, are found in calcareous claystone, calcareous mudstones and argillaceous mudstones

(from Asbian to Pendleian; Figs. 1 and 2); contain high organic matter richness (TOC_o ; 3.78 to 11.16 wt%; average 5.83 wt%); have high pyrolysate yield (7.63 to 32.60; average 15.66); have low production indices (0.07 to 0.12; average 0.09); have moderate hydrogen indices (HI_o ; 253 to 505; average 389); and contain predominantly Type II/III kerogen (constrained by transmitted white light observations; a significant portion of Type I kerogen is also assigned when data based on autofluorescence properties of the kerogen fraction is included; Tables 1, 2 and 3). These results demonstrate that organofacies A and intermediate, when sufficiently thermally mature, do have the potential to be a good source rock reservoir but the kerogen type (containing significant proportion of AOM/Type I and Type II) suggests that primary generation may result in higher oil yields rather than gas, but secondary gas generational potential is likely to be significant similar to that described by Yang et al. (2015). However, the studied interval is not thermally mature and as such, it cannot be considered prospective but holds key information to predict prospective intervals within contemporaneous successions within the Bowland Basin, which have reached the thermal maturity required. In addition, these results highlight areas for future work including verifying whether the ORFA method is more generally applicable for samples over a range of thermal maturities (e.g., vitrinite reflectance range of 0.4 to 2.0 R_o) and evaluating whether the ORFA method could be improved by using a distribution of E_a and A values rather than treating the pre-exponential factor (A) as a constant.

CONCLUSIONS

1. Two-end-member organofacies were determined based on the abundance of the 56 kcal/mol activation energy peak derived from One-Run-Fixed-Arrhenius kerogen kinetic analysis: an absence (or < 5%) indicating 'organofacies A' which contains the highest proportion of algal material and therefore Type I kerogen; and a presence (> 15%) indicating 'organofacies B' which contains the highest proportion of spore-morphs and therefore Type II kerogen. These organofacies are broadly equivalent to previously described marine organic facies: AB and BC of Tyson (1995) and organic

facies B/C and B/E of Evenick and McCain (2013), respectively.

2. In addition to the two-end-member organofacies, a mixed or 'intermediate organofacies' with a 5 to 15% 56 kcal/mol activation energy abundance was also identified; these samples contain mixed characteristics of both organofacies A and B. The occurrence of the intermediate organofacies is hypothesized to result from mixing and dilution between the two-end-member facies, organofacies A and B.
3. The depositional environment determined from an APP plot for organofacies A occurs between the shelf edge to slope to basin, while organofacies B occur only within the lower slope; all organofacies occur within a dysoxic to anoxic sedimentary system. These findings support the conclusions drawn by Newport et al. (2017) based on sedimentological evidence: with organofacies A lithofacies representing deposition from dilute waning density flows and background hemipelagic suspension settling; and organofacies B lithofacies representing deposition from dilute waning density flows and deposition from low-strength cohesive debrites.
4. Prospectivity of the Bowland Shale Formation when sufficiently thermally mature does have the potential to be a good source rock reservoir but due to significant Type I and II kerogen proportions intervals may result in primary generation of oil, but secondary gas generation potential is likely to be larger than primary gas generation.
5. This study demonstrates that in determining organic matter quality and quantity One-Run-Fixed-Arrhenius kerogen kinetic analysis does provide comparable net results to that of palynological analysis. This is significant as ORFA data are less labor intensive than palynological studies and can be collected using existing Rock-Eval data; therefore, enabling cheaper and faster organic characterization to be available to geoscientists during initial source rock appraisal. However, caution must be exercised in drawing interpretations as to biological source(s), OM mixing and preservation state(s) without additional investigation using data derived from detailed palynological analysis.

ACKNOWLEDGMENTS

S.M.N. thanks Natural Environment Research Council (NERC) EAO Doctoral Training Partnership for provision of funding (NE/L002469/1) for this PhD research and the AAPG Grant-In-Aid program for the John H. and Colleen Silcox Named Grant funds received. The authors thank M. Jones at Newcastle University, G. Hansen at APT Norway and D. Waples at Sirius Exploration Geochemistry Inc. for analytical services provided, as well as the British Geological Survey for the loan of material. Jane Flint is thanked for the preparation of the palynological slides. E.H. and J.H. publish with the approval of the Executive Director of the British Geological Survey, Natural Environment Research Council. We would also like to thank Paul C. Hackley for his comments and suggestions on an earlier draft of this work.

OPEN ACCESS

This article is distributed under the terms of the Creative Commons Attribution 4.0 International License (<http://creativecommons.org/licenses/by/4.0/>), which permits unrestricted use, distribution, and reproduction in any medium, provided you give appropriate credit to the original author(s) and the source, provide a link to the Creative Commons license, and indicate if changes were made.

ELECTRONIC SUPPLEMENTARY MATERIAL

The online version of this article (<https://doi.org/10.1007/s11053-019-09543-z>) contains supplementary material, which is available to authorized users.

REFERENCES

- Aitkenhead, N., Bridge, D., Riley, N. J., Kimbell, S. F., Evans, D. J., & Humphreys, B. (1992). *Geology of the country around Garstang*. London: Memoir of the British Geological Survey, Sheet 67 (England & Wales).
- Andrews, I. J. (2013). *The Carboniferous Bowland Shale gas study: Geology and resource estimation*. London: British Geological Survey for Department of Energy and Climate Change.
- Aplin, A. C., & Macquaker, J. H. S. (2011). Mudstone diversity: Origin and implications for source, seal, and reservoir properties in petroleum systems. *AAPG Bulletin*, 95, 2031–2059.
- Arthurton, R. S., Johnson, E. W., & Mundy, D. J. C. (1988). *Geology of the country around settle*. London: Memoir of the British Geological Survey.
- Behar, F., Kressmann, S., Rudkiewicz, J. L., & Vandenbroucke, M. (1992). Experimental simulation in a confined system and kinetic modelling of kerogen and oil cracking. *Organic Geochemistry*, 19, 173–189.
- Behar, F., Vandenbroucke, M., Tang, Y., Marquis, F., & Espitalie, J. (1997). Thermal cracking of kerogen in open and closed systems: Determination of kinetic parameters and stoichiometric coefficients for oil and gas generation. *Organic Geochemistry*, 26, 321–339.
- Bernard, S., Horsfield, B., Schulz, H. M., Wirth, R., Schreiber, A., & Sherwood, N. (2012). Geochemical evolution of organic-rich shales with increasing maturity: A STXM and TEM study of the Posidonia Shale (Lower Toarcian, northern Germany). *Marine and Petroleum Geology*, 31, 70–89.
- Brandon, A., Aitkenhead, N., Crofts, R. G., Ellison, R. A., Evans, D. J., & Riley, N. J. (1998). *Geology of the country around Lancaster*. London: Memoir of the British Geological Survey, Sheet 59.
- Burnham, A. K., Braun, R. L., & Samoun, A. M. (1988). Further comparison of methods for measuring kerogen pyrolysis rates and fitting kinetic parameters. *Organic Geochemistry*, 13, 839–845.
- Charpentier, B. R. R., & Cook, T. A. (2011). USGS methodology for assessing continuous petroleum resources (No. 2011-1167). US Geological Survey.
- Clarke, H., Turner, P., Bustin, R. M., Riley, N., & Besly, B. (2018). Shale gas resources of the Bowland Basin, NW England: A holistic study. *Petroleum Geoscience*, 24(3), 287–322.
- Cornford, C., Rullkotter, J., & Welte, D. (1980). A synthesis of organic petrographic and geochemical results from DSDP sites in the eastern central North Atlantic. *Physics and Chemistry of the Earth*, 12, 445–453.
- Creaney, S., & Passey, Q. R. (1993). Recurring patterns of total organic carbon and source rock quality within a sequence stratigraphic framework. *AAPG Bulletin*, 77, 386–401.
- Davies, S. J. (2008). The record of Carboniferous sea-level change in low-latitude sedimentary successions from Britain and Ireland during the onset of the late Paleozoic ice age. *Geological Society of America Special Papers*, 441, 187–204.
- Davies, S. J., & McLean, D. (1996). Spectral gamma-ray and palynological characterization of Kinderscoutian marine bands in the Namurian of the Pennine Basin. *Proceedings of the Yorkshire Geological Society*, 51, 103–114, <https://doi.org/10.1144/pygs.51.2.103>.
- Durand, B. (1980). *Kerogen. Insoluble organic matter from sedimentary rocks*. Paris: Éditions Technip.
- Durand, B., & Espitalié, J. (1973). Evolution de la matière organique au cours de l'enfouissement des sédiments. *Compte rendu de l'Académie des Sciences (Paris)*, 276, 2253–2256.
- Durand, B., & Monin, J. C. (1980). Elemental analysis of kerogens. In B. Durand (Ed.), *Kerogen, insoluble organic matter from sedimentary rocks* (pp. 113–142). Paris: Editions Technip.
- Espitalié, J., Madec, M., Tissot, B. P., Mennig, J. J., & Leplat, P. (1977). Source rock characterization method for petroleum exploration. *Paper OTC (Offshore Technology Conference)*, 2935, 439–444.
- Evenick, J. C., & McCain, T. (2013). Method for characterizing source rock organofacies using bulk rock composition. In J.-Y. Chatellier & D. M. Jarvie (Eds.), *AAPG Memoir 103: Critical assessment of shale resource plays* (pp. 71–80). Tulsa, OK: AAPG.
- Fishman, N. S., Hackley, P. C., Lowers, H. A., Hill, R. J., Egenhoff, S. O., Eberl, D. D., et al. (2012). The nature of porosity in organic-rich mudstones of the Upper Jurassic Kimmeridge

- Clay Formation, North Sea, offshore United Kingdom. *International Journal of Coal Geology*, 103, 32–50.
- Fraser, A. J., & Gawthorpe, R. L. (1990). Tectono-stratigraphic development and hydrocarbon habitat of the Carboniferous in northern England. In R. F. P. Hardman & J. Brooks (Eds.), *Tectonic events responsible for Britain's oil and gas reserves* (pp. 49–86). London: Geological Society of London.
- Fraser, A. J., & Gawthorpe, R. L. (2003). *An atlas of Carboniferous basin evolution in northern England*. Geological Society Memoirs 28 London: Geological Society of London.
- Gawthorpe, R. L. (1986). Sedimentation during carbonate ramp-to-slope evolution in a tectonically active area: Bowland Basin (Dinantian), northern England. *Sedimentology*, 33, 185–206.
- Gawthorpe, R. L. (1987). Tectono-sedimentary evolution of the Bowland Basin, N England, during the Dinantian. *Journal of the Geological Society, London*, 144, 59–71.
- Gilman, J., & Robinson, C. (2011). Success and failure in shale gas exploration and development: Attributes that make the difference. In *AAPG international conference and exhibition, Calgary, Alberta, Canada September 12–15*, p. 31.
- Hackley, P. C., & Cardott, B. J. (2016). Application of organic petrography in North American shale petroleum systems: A review. *International Journal of Coal Geology*, 163, 8–51.
- Hennissen, J. A. I., Hough, E., Vane, C. H., Leng, M. J., Kemp, S. J., & Stephenson, M. H. (2017). The prospectivity of a potential shale gas play: An example from the southern Pennine Basin (central England, UK). *Marine and Petroleum Geology*, 86, 1047–1066.
- Horsfield, B., Disko, U., & Leistner, F. (1989). The micro-scale simulation of maturation: Outline of a new technique and its potential applications. *Geologische Rundschau*, 78, 361–373.
- Hough, E., Vane, C. H., Smith, N. J. P., & Moss-Hayes, V. L. (2014). The Bowland Shale in the Roosecote Borehole of the Lancaster fells sub-basin, Craven Basin, UK: A potential UK shale gas play? In *SPE/EAGE European unconventional conference and exhibition*, pp. 25–27.
- Jarvie, D. M. (2012). Shale resource systems for oil and gas: Part 1—Shale-gas resource systems. In J. A. Breyer (Ed.), *Shale reservoirs—Giant resources for the 21st century: AAPG Memoir 97* (pp. 69–87). Tulsa, OK: American Association of Petroleum Geologists.
- Jarvie, D. M., Hill, R. J., Ruble, T. E., & Pollastro, R. M. (2007). Unconventional shale-gas systems: The Mississippian Barnett Shale of north-central Texas as one model for thermogenic shale-gas assessment. *AAPG Bulletin*, 91, 475–499.
- Jones, R. W. (1987). Organic Facies. In J. Brooks & D. H. Welte (Eds.), *Advances in petroleum geochemistry* (pp. 1–90). London: Academic Press.
- Jones, R. W., & Demaison, G. J. (1982). Organic facies-stratigraphic concept and exploration tool. In A. Sadivar-Sali (Ed.), *Proceedings 2nd ASCOPE conference and exhibition* (pp. 51–68). Manila: Asian Council on Petroleum.
- Kane, I. A., Catterall, V., McCaffrey, W. D., & Martinsen, O. J. (2010). Submarine channel response to intrabasinal tectonics: The influence of lateral tilt. *AAPG Bulletin*, 94, 189–219.
- Katz, B. J. (1995). A survey of rift basin source rocks. *Geological Society, London, Special Publications*, 80, 213–240.
- Kirby, G. A., Baily, H. E., Chadwick, R. A., Evans, D. J., Holliday, D. W., Holloway, S., et al. (2000). *The structure and evolution of the Craven Basin and adjacent areas*. London: Subsurface Memoir of the British Geological Survey.
- Lakshmanan, C. C., Bennett, M. L., & White, N. (1991). Implications of multiplicity in kinetic parameters to petroleum exploration: Distributed activation energy models. *Energy & Fuels*, 5, 110–117.
- Lazar, O. R., Bohacs, K., Schieber, J., Macquaker, J., & Demko, T. (2015). In G. J. Nichols, B. Ricketts, & M. Tomlinson (Eds.), *Mudstone primer: Lithofacies variations, diagnostic criteria, and sedimentological/stratigraphical implications at Lamina to Bedset Scale (SEPM Concepts in Sedimentology and Paleontology #12)* (pp. 3–16). Tulsa, OK: SEPM.
- Lewan, M. D., & Ruble, T. E. (2002). Comparison of petroleum generation kinetics by isothermal hydrous and nonisothermal open-system pyrolysis. *Organic Geochemistry*, 33, 1457–1475.
- Lewan, M. D., Winters, J. C., & McDonald, J. H. (1979). Generation of oil-like pyrolyzates from organic-rich shales. *Science*, 203, 897–900.
- Lin, R., & Davis, R. (1988). *Chemistry of coal maceral fluorescence: With special reference to the huminite/vitrinite group*. University Park, PA: Pennsylvania State University.
- Macquaker, J. H. S., Taylor, K. G., Keller, M., & Polyá, D. (2014). Compositional controls on early diagenetic pathways in fine-grained sedimentary rocks: Implications for predicting unconventional reservoir attributes of mudstones. *AAPG Bulletin*, 3, 587–603.
- Maher, L. J. (1981). Statistics for microfossil concentration measurements employing samples spiked with marker grains. *Review of Palaeobotany and Palynology*, 32, 153–191.
- Metcalfe, I., & Riley, N. J. (2010). Conodont Colour Alteration pattern in the Carboniferous of the Craven Basin and adjacent areas, northern England. *Proceedings of the Yorkshire Geological Society*, 58, 1–8.
- Newport, S. M., Jerrett, R. M., Taylor, K. G., Hough, E., & Worden, R. H. (2017). Sedimentology and microfacies of a mud-rich slope succession: In the Carboniferous Bowland Basin, NW England (UK). *Journal of the Geological Society, London*, 175, 16.
- Nielsen, S. B., & Dahl, B. (1991). Confidence limits on kinetic models of primary cracking and implications for the modelling of hydrocarbon generation. *Marine and Petroleum Geology*, 8, 483–492.
- Nordeng, S. H. (2015). Compensating for the compensation effect using simulated and experimental kinetics from the Bakken and Red River Formations, Williston Basin, North Dakota. In *AAPG annual convention and exhibition, Denver, Colorado, May 31–June 3*, p. 24.
- Owens, B. (2004). A revised palynozonation of British Namurian deposits and comparisons with eastern Europe. *Micropaleontology*, 50, 89–103. <https://doi.org/10.2113/50.1.89>.
- Passey, Q. R., Creaney, S., Kulla, J. B., Moretti, F. J., & Stroud, J. D. (1990). A practical model for organic richness from porosity and resistivity logs. *AAPG Bulletin*, 74, 1777–1794.
- Pepper, A. S., & Corvi, P. J. (1995). Simple kinetic models of petroleum formation. Part I: Oil and gas generation from kerogen. *Marine and Petroleum Geology*, 12, 291–319.
- Peters, K. E., Burnham, A. K., & Walters, C. C. (2015). Petroleum generation kinetics: Single versus multiple heating ramp open-system pyrolysis. *AAPG Bulletin*, 99, 591–616.
- Peters, K. E., & Cassa, M. R. (1994). Applied source rock geochemistry. In L. B. Magoon & W. G. Dow (Eds.), *AAPG Memoir 60: The petroleum system—From source to trap* (pp. 93–120). AAPG: Tulsa, OK.
- Raiswell, R., & Berner, R. A. (1987). Organic carbon losses during burial and thermal maturation of normal marine shales. *Geology*, 15, 853–856.
- Riegel, W. (2008). The Late Palaeozoic phytoplankton black-out—Artefact or evidence of global change? *Review of Palaeobotany and Palynology*, 148, 73–90.
- Riley, N. J. (1988). *Stratigraphy of BP minerals borehole MHD11, Marl Hill, Whitewell, Lancs*. Technical report WH/PD/88/304R.
- Riley, N. J. (1990). Stratigraphy of the Worston Shale Group (Dinantian), Craven Basin, north-west England. *Proceedings of the Yorkshire Geological Society*, 48, 163–187.
- Riley, N. J. (1993). Dinantian (Lower Carboniferous) biostratigraphy and chronostratigraphy in the British Isles. *Journal of the Geological Society*, 150, 427–446.

- Ritter, U., Myhr, M. B., Vinge, T., & Aareskjold, K. (1995). Experimental heating and kinetic models of source rocks: Comparison of different methods. *Organic Geochemistry*, 23, 1–9.
- Robert, P. (1988). *Organic metamorphism and geothermal history. Microscopic study of organic matter and thermal evolution of sedimentary basins*. Dordrecht: Elf-Aquitain and D. Reidel Publishing.
- Roger, M. A. (1979). Application of organic facies concepts to hydrocarbon source rock evaluation. In *10th world petroleum congress: Bucharest, Romania*, p. 8.
- Ross, D. J. K., & Bustin, R. M. (2008). Characterizing the shale gas resource potential of Devonian—Mississippian strata in the Western Canada sedimentary basin: Application of an integrated formation evaluation. *AAPG Bulletin*, 92, 87–125.
- Ross, D. J. K., & Bustin, R. M. (2009). The importance of shale composition and pore structure upon gas storage potential of shale gas reservoirs. *Marine and Petroleum Geology*, 26, 916–927.
- Schenk, H. J., & Horsfield, B. (1993). Kinetics of petroleum generation by programmed-temperature closed-versus open-system pyrolysis. *Geochimica et Cosmochimica Acta*, 57, 623–630.
- Schieber, J. (2016). Experimental testing of the transport-durability of shale lithics and its implications for interpreting the rock record. *Sedimentary Geology*, 331, 162–169.
- Schieber, J., Southard, J. B., & Schimmelmann, A. (2010). Lenticular shale fabrics resulting from intermittent erosion of water-rich muds—Interpreting the rock record in the light of recent flume experiments. *Journal of Sedimentary Research*, 80, 119–128.
- Servais, T., Martin, R. E., & Nutzal, A. (2016). The impact of the ‘terrestrialisation process’ in the late Palaeozoic: pCO₂, pO₂, and the ‘phytoplankton blackout’. *Review of Palaeobotany and Palynology*, 224, 26–37.
- Somerville, I. D. (2008). Biostratigraphic zonation and correlation of Mississippian rocks in Western Europe: Some case studies in the late Viséan/Serpukhovian. *Geological Journal*, 43, 209–240, <https://doi.org/10.1002/gj.1097>.
- Stockmarr, J. (1971). Tablets with spores used in absolute pollen analysis. *Pollen et Spores*, 13, 615–621.
- Talling, P. J., Masson, D. G., Sumner, E. J., & Malgesini, G. (2012). Subaqueous sediment density flows: Depositional processes and deposit types. *Sedimentology*, 59, 1937–2003.
- Tissot, B. P., Durand, B., Espitalié, J., & Combaz, A. (1974). Influence of nature and diagenesis of organic matter in formation of petroleum. *AAPG Bulletin*, 58, 506.
- Tissot, B. P., & Espitalié, J. (1975). L'évolution thermique de la matière organique des sédiments: applications d'une simulation mathématique. Potentiel pétrolier des bassins sédimentaires de reconstitution de l'histoire thermique des sédiments Thermal Evolution of Organic Matter in Sedime. *Review of the Institute Français Petroleum*, 30, 743–778.
- Tissot, B. P., & Welte, D. H. (1984). *Petroleum formation and occurrence: A new approach to oil and gas exploration* (2nd ed.). Berlin: Springer.
- Tribouillard, N. P., & Gorin, G. E. (1991). Organic facies of the early Albian Niveau Paquier, a key black shales horizon of the Marnes Bleues formation in the Vocontian Trough (Subalpine Ranges, SE France). *Palaeogeography, Palaeoclimatology, Palaeoecology*, 85, 227–237.
- Tuweni, A. O., & Tyson, R. V. (1994). Organic facies variations in the Westbury Formation (Rhaetic, Bristol channel, SW England). *Organic Geochemistry*, 21, 1001–1014.
- Tyson, R. V. (1987). The genesis and palynofacies characteristics of marine petroleum source rocks. In J. Brooks & A. J. Fleet (Eds.), *Marine petroleum source rocks: Geological Society Special Publication No. 26* (pp. 47–67). London: Geological Society of London.
- Tyson, R. V. (1995). *Sedimentary organic matter*. Dordrecht: Springer. <https://doi.org/10.1007/978-94-011-0739-6>.
- Tyson, R. V. (2004). Variation in marine total organic carbon through the type Kimmeridge Clay Formation (Late Jurassic), Dorset, UK. *Journal of the Geological Society*, 161, 667–673.
- Tyson, R. V. (2006). Calibration of hydrogen indices with microscopy: A review, reanalysis and new results using the fluorescence scale. *Organic Geochemistry*, 37, 45–63.
- van Krevelen, D. W. (1961). *Coal: Typology—Chemistry—Physics—Constitution* (1st ed.). Amsterdam: Elsevier.
- Vandenbroucke, M., & Largeau, C. (2007). Kerogen origin, evolution and structure. *Organic Geochemistry*, 38, 719–833.
- Waples, D. W. (2000). The kinetics of in-reservoir oil destruction and gas formation: Constraints from experimental and empirical data, and from thermodynamics. *Organic Geochemistry*, 31, 553–575.
- Waples, D. W. (2016). Discussion and reply: Petroleum generation kinetics: Single versus multiple heating ramp open-system pyrolysis. *AAPG Bulletin*, 100, 683–689.
- Waples, D. W., & Nowaczewski, V. S. (2013). Source-rock kinetics. <https://siriusdummy.files.wordpress.com/2013/11/percentage-on-sr-kinetics.pdf>. Accessed 27 Mar 2017.
- Waples, D. W., Vera, A., & Pacheco, J. (2002). A new method for kinetic analysis of source rocks: Development and application as a thermal and organic facies indicator in the Tithonian of the Gulf of Campeche, Mexico. In *8th Latin American congress on organic geochemistry, Cartagena, Colombia, October 20–24*, pp. 296–298.
- Waters, C. N., & Condon, D. J. (2012). Nature and timing of Late Mississippian to Mid Pennsylvanian glacio-eustatic sea-level changes of the Pennine Basin, UK. *Journal of the Geological Society*, 169, 37–51.
- Waters, C. N., Somerville, I. D., Jones, N. S., Cleal, C. J., Collinson, J. D., Waters, R. A., et al. (2011). *A revised correlation of carboniferous rocks in the British Isles: Special Report No. 26*. London: The Geological Society.
- Waters, C. N., Waters, R. A., Barclay, W. J., & Davies, R. J. (2009). A Lithostratigraphical Framework for the Carboniferous Successions of Southern Great Britain (Onshore), RR/09/01.
- Weiss, H. M., Wilhelms, A., Mills, N., Scotchmer, J., Hall, P. B., Lind, K., & Brekke, T. (2000). NIGOGA: The Norwegian industry guide to organic geochemical analyses. In *NIGOGA: The Norwegian industry guide to organic geochemical analyses*, vol. 102, 4th edn. World Wide Web Address, <http://www.npd.no/engelsk/nigoga/default.htm>. Accessed 13 July 2018.
- Wood, D. A. (2019). Advances in establishing credible reaction-kinetics distributions to fit and explain multi-heating rate S₂ pyrolysis peaks of kerogens and shales. *Advances in Geo-Energy Research*, 3, 1–28.
- Yang, S., Horsfield, B., Mahlstedt, N., Stephenson, M., & Köntzner, S. (2015). On the primary and secondary petroleum generating characteristics of the Bowland Shale, northern England. *Journal of the Geological Society*, 173(2), 292–305. <https://doi.org/10.1144/jgs2015-056>.